Post Pulse Compression & Partially Adaptive Multi-Waveform STAP

Lumumba A. Harnett [1*], Justin G. Metcalf [2], Shannon D. Blunt [3]

[1] Radar Systems Lab (RSL), University of Kansas, Lawrence, KS, USA, and Radar Division, Naval Research Laboratory (NRL), Washington, DC, USA.

[2] School of Electrical and Computer Engineering, Advanced Radar Research Center, University of Oklahoma, Norman, OK USA, previously Sensors Directorate, US Air Force Research Laboratory (AFRL), Wright-Patterson AFB, Dayton, OH, USA.

[3] Radar Systems Lab (RSL), University of Kansas, Lawrence, KS, USA
*LHarnett@ku.edu

Abstract: The recently developed multi-waveform (MuW) space-time adaptive processing (or μ-STAP) formulation incorporates additional training data into the sample covariance matrix estimate by applying multiple different secondary pulse compression filters to the raw received data, where these filters have a relatively low cross-correlation with the transmitted waveform. The inclusion of this additional training data has been shown to improve robustness to non-homogeneous clutter due to a "range smearing" homogenizing effect of the secondary filters. Here we introduce Post μ-STAP (Pμ-STAP), a new form of μ-STAP that similarly generates additional training data, albeit after pulse compression has already occurred. In addition, we combine Pμ-STAP with well-known partially adaptive STAP techniques to assess whether the enhanced performance is retained for reduced-dimension operation. Specifically, element-space post-Doppler, beam-space pre-Doppler, and beam-space post-Doppler implementations of Pμ-STAP are evaluated via SINR analysis and minimum detectable Doppler for different simulated clutter environments.

1. Introduction

Airborne ground moving target indication (GMTI) radar must combat angle-Doppler coupled clutter caused by platform motion. Space-time adaptive processing (STAP) generates a joint angle-Doppler filter to suppress this coupled clutter and interference for subsequent detection of moving targets. For each range/Doppler cell-under-test (CUT) a unique filter is formed via estimation of the associated clutter/ interference covariance matrix under the assumption that the training data used to form the matrix is independent and identically distributed (IID) [1]. The IID assumption implies that the clutter is stationary and homogeneous, and under this condition the STAP filter realized by the sample covariance matrix (SCM) estimate approaches the optimal filter, in a maximum signal-to-interference-plus-noise ratio (SINR) sense, as the number of training data samples increases [3, 4].

However, in the presence of non-homogeneous clutter, STAP techniques can suffer severe degradation in SINR due to a variety of reasons [5] including insufficient sample support (of IID training data), contamination of the training data by targets of interest (leading to self-cancellation issues), and CUT clutter discretes that are not represented in the SCM. With the additional inclusion of practical effects such as internal clutter motion, aircraft crabbing, and channel mismatch [6], accurate estimation of the STAP SCM remains a difficult problem.

Over the years numerous robust solutions have been proposed for this problem (e.g. [5, 7-30]) with varying trade-offs, assumptions, and degrees of success. A prominent trend among these is the down-selection/modification of the training data itself as a means to achieve improved homogeneity [8-11, 15, 16, 18, 20, 21, 24, 26, 27]. In a bit of a departure from these methods, the recently developed μ-STAP formulation [28-30] involves the generation of *additional* training data via the application of multiple pulse compression filters that possess relatively low cross-correlation with the actual emitted waveform. Because this new training data involves different mixtures (in range) of the same data, it clearly does not produce new independent snapshots. However, the range-domain "smearing" effect that occurs when applying these other filters provides a degree of training data homogenization that has been shown to be beneficial for non-homogeneous clutter [28-30]. Further, it should be noted that this process of generating additional smeared training data can be readily combined with other robust STAP techniques such as those cited above.

Of course, legacy radar systems that perform pulse compression before analog-to-digital conversion would not benefit from the homogenization effect provided by μ-STAP since this formulation operates on the raw received data prior to pulse compression. Consequently,

This work was supported in part by a subcontract with Matrix Research, Inc. for research sponsored by AFRL under Prime Contract No. FA8650-14-D-1722, by the NSF Graduate Research Fellowship Program under Grant No. DGE-1451148, and by the University of Kansas Chancellor's Fellowship.

a new form of μ-STAP called *Post* μ-STAP (Pμ-STAP) is introduced here to generate additional training data and perform homogenization after pulse compression has occurred.

For a radar with N antenna array elements, M pulses in the coherent processing interval (CPI), and assuming homogeneous clutter, the standard rule is that at least $2NM$ independent space-time snapshots are required to estimate the SCM within 3 dB of the optimum (in terms of average SINR) [2]. This required number of snapshots is even higher if the training data is non-homogeneous [5, 31, 32]. For typical array sizes and CPI lengths, it is generally not feasible to expect the availability of $2NM$ or greater IID training data samples. Likewise, the associated SCM of dimensionality $NM \times NM$ may incur too high a computational cost to invert, particularly since multiple SCM estimates are necessary and the result must be obtained at or near real-time. Thus a variety of different partially adaptive and reduced-rank techniques have been developed (see [3, 4] for an overview).

Here Pμ-STAP is also evaluated in the context of partially adaptive implementations [3]. Specifically, we examine element-space post-Doppler (previously considered for μ-STAP in [33]), beam-space pre-Doppler, and beam-space post-Doppler. These reduced dimension implementations of Pμ-STAP are assessed relative to optimal SINR (given clairvoyant knowledge of the covariance matrix) and minimum detectable Doppler (i.e. relative velocity).

2. Multi-Waveform STAP

In [30] two forms of μ-STAP were considered: a multiple-input multiple-output (MIMO) mode in which lower power secondary waveforms were emitted in directions other than the primary mainbeam direction, and a single-input multiple-output (SIMO) mode in which one waveform is emitted yet multiple different pulse compression filters are applied on receive. While the former may provide somewhat better sidelobe clutter rejection due to waveform separability, it is also a more complex hardware implementation. In contrast, the SIMO mode emission structure is no different from standard GMTI and thus requires no transmit hardware modifications. Because it is more widely applicable and easier to realize, we shall focus on the SIMO mode here, though these results should be directly extensible to the MIMO mode as well.

For SIMO μ-STAP, consider an airborne pulse-Doppler radar transmitting a CPI of M pulses modulated with a single waveform in a given spatial direction θ_{look} via an N element uniform linear array (ULA) antenna. The received response from the illuminated scattering and noise for the mth pulse and nth antenna element is thus

$$y(m,n,t) = \sum_{\omega}\sum_{\theta}\left[s(t) * x(t,\omega,\theta,\theta_{\text{look}})\right]e^{j(m\omega+n\theta)} + v(t) \quad (1)$$

where $*$ denotes convolution, $s(t)$ is the transmitted waveform, $v(t)$ is additive noise, and $x(t, \omega, \theta, \theta_{\text{look}})$ is the induced scattering impinging on the array as a function of Doppler ω, spatial angle θ, and the direction of illumination θ_{look}.

Denote $h_{\text{prime}}(t)$ as the primary pulse compression filter, which is a matched filter (or possible mismatched filter) for transmitted waveform $s(t)$. The SIMO version of μ-STAP [30] additionally defines the set of "unmatched" secondary pulse compression filters $h_{\text{sec},k}(t)$ for $k = 1, 2, \ldots, K$ that possess a relatively low cross-correlation with the transmitted waveform. Where the matched filter provides a range-focused estimate of the radar scattering, the low cross-correlation responses produced by the secondary filters alternatively realize a smearing of the scattering in range that helps to homogenize the non-homogeneities of clutter discretes and targets contaminating the training data. These $K + 1$ pulse compression responses can collectively be expressed as

$$\begin{aligned} z_{\text{prime}}(m,n,t) &= h_{\text{prime}}(t) * y(m,n,t) \\ z_{\text{sec},1}(m,n,t) &= h_{\text{sec},1}(t) * y(m,n,t) \\ z_{\text{sec},2}(m,n,t) &= h_{\text{sec},2}(t) * y(m,n,t) \\ &\vdots \\ z_{\text{sec},K}(m,n,t) &= h_{\text{sec},K}(t) * y(m,n,t) \end{aligned} \quad (2)$$

for the $n = 0, 1, \ldots, N-1$ antenna elements in a ULA and $m = 0, 1, \ldots, M-1$ pulses in the CPI. Discretising these filter outputs and collecting the MN samples for each ℓth range index into a vector produces $K + 1$ space-time snapshots denoted as $\mathbf{z}_{\text{prime}}(\ell)$ and $\mathbf{z}_{\text{sec},k}(\ell)$ for $k = 1, 2, \ldots, K$. Note that the order of receive filtering in (2) and discretization could clearly be reversed as well.

Generally speaking, for a given spatial illumination direction θ_{look} and Doppler frequency ω_{D}, a space-time adaptive filter $\mathbf{w}(\ell_{\text{CUT}}, \theta_{\text{look}}, \omega_{\text{D}})$ is generated and applied to each candidate CUT as

$$\alpha(\ell_{\text{CUT}}, \omega_{\text{D}}) = \mathbf{w}^H(\ell_{\text{CUT}}, \theta_{\text{look}}, \omega_{\text{D}})\, \mathbf{z}_{\text{prime}}(\ell_{\text{CUT}}). \quad (3)$$

The filter response $\alpha(\ell_{\text{CUT}}, \omega_{\text{D}})$ can then be evaluated by a detector to determine if a moving target is present at the specified range and Doppler. The STAP filter that optimizes SINR is determined via

$$\mathbf{w}(\ell_{\text{CUT}}, \theta_{\text{look}}, \omega_{\text{D}}) = \mathbf{R}^{-1}(\ell_{\text{CUT}})\, \mathbf{c}_{\text{st}}(\theta_{\text{look}}, \omega_{\text{D}}), \quad (4)$$

where $\mathbf{R}(\ell_{\mathrm{CUT}})$ is the covariance matrix of the clutter and interference in the CUT, and the space-time steering vector

$$\mathbf{c}_{\mathrm{st}}(\theta_{\mathrm{look}}, \omega_{\mathrm{D}}) = \mathbf{c}_{\mathrm{t}}(\omega_{\mathrm{D}}) \otimes \mathbf{c}_{\mathrm{s}}(\theta_{\mathrm{look}}) \tag{5}$$

is formed by the Kronecker product of the individual temporal and spatial steering vectors [3].

The clutter and interference covariance matrix is usually estimated using the sample data surrounding the CUT under the assumption that this data is statistically homogeneous with the CUT snapshot. Notwithstanding the variety of ways in which training data can be modified/down-selected (e.g. [8-11, 15, 16, 18, 20, 21, 24, 26, 27]), the standard SCM estimate is obtained as

$$\hat{\mathbf{R}}_{\mathrm{prime}}(\ell_{\mathrm{CUT}}) = \frac{1}{n(L_{\mathrm{prime}})} \sum_{\substack{\ell \in L_{\mathrm{prime}} \\ \ell \neq \ell_{\mathrm{CUT}} \pm G}} \mathbf{z}_{\mathrm{prime}}(\ell)\, \mathbf{z}_{\mathrm{prime}}^{H}(\ell) \tag{6}$$

using the set of primary snapshots in L_{prime} with cardinality $n(L_{\mathrm{prime}})$. The exclusion of range indices $\ell_{\mathrm{CUT}} \pm G$ comprising the CUT and surrounding guard cells from the training data is generally used to avoid including possible moving targets in/near the CUT.

The problem with the SCM estimate of (6) is that it may not be an accurate reflection of the true covariance matrix due to all the reasons discussed in the previous section. To further supplement the many robust SCM estimators that have been developed (e.g. [5, 7-27]), the SIMO μ-STAP formulation in [30] proposed the use of additional training data obtained from the K secondary filters in (2). For example, a "no primary" (NP) μ-STAP form of SCM based only on secondary training data can be realized as

$$\hat{\mathbf{R}}_{\mu,\mathrm{NP}}(\ell_{\mathrm{CUT}}) = \frac{1}{n(L_{\mathrm{prime}})K} \sum_{k=1}^{K} \sum_{\ell \in L_{\mathrm{prime}}} \mathbf{z}_{\mathrm{sec},k}(\ell)\, \mathbf{z}_{\mathrm{sec},k}^{H}(\ell) \tag{7}$$

which does not exclude the CUT or guard cells, as doing so is pointless because of the range-smearing effect of the secondary filters. The homogenized SCM from (7) can also be combined with the traditional SCM from (6) to form the μ-STAP SCM

$$\hat{\mathbf{R}}_{\mu}(\ell_{\mathrm{CUT}}) = \hat{\mathbf{R}}_{\mathrm{prime}}(\ell_{\mathrm{CUT}}) + \hat{\mathbf{R}}_{\mu,\mathrm{NP}}(\ell_{\mathrm{CUT}})\,. \tag{8}$$

Diagonal loading is often used with the standard SCM in (6) by adding $\sigma_v^2 \mathbf{I}_{MN}$, for σ_v^2 the noise power and $\mathbf{I}_{NM}$ an $NM \times NM$ identity matrix. This structure can likewise be used with the μ-STAP SCMs in (7) and (8). It was shown analytically and via Monte Carlo simulation in [30] that the μ-STAP SCMs improve robustness to a variety of nonhomogeneous clutter structures.

2.1. Post Pulse Compression Multi-Waveform STAP

In its current form, μ-STAP operates on the raw received signal $y(m, n, t)$, or its discretized form, prior to pulse compression to generate the $K + 1$ responses in (2). However, for legacy systems such as those using stretch processing on receive, this raw data is not readily available.

To that end, a new variant of μ-STAP denoted as *Post μ-STAP* (Pμ-STAP) is proposed that likewise realizes a set of range-smeared secondary data, albeit through manipulation of the primary data after pulse compression has already occurred. Since the pulse compressed data possesses a range-focused response due to matched filtering relative to the transmitted waveform, Pμ-STAP involves the application of subsequent *homogenization filters* to smear this match filtered response in range, and in so doing obtain essentially the same improved robustness to non-homogeneous clutter as μ-STAP.

In this arrangement the discretised version of the primary pulse compression response from the top line of (2) is then filtered as

$$\begin{aligned}
\rho_{\mathrm{prime}}(m,n,\ell) &= g_{\mathrm{prime}}(\ell) * z_{\mathrm{prime}}(m,n,\ell) \\
\rho_{\mathrm{sec},1}(m,n,\ell) &= g_{\mathrm{sec},1}(\ell) * z_{\mathrm{prime}}(m,n,\ell) \\
\rho_{\mathrm{sec},2}(m,n,\ell) &= g_{\mathrm{sec},2}(\ell) * z_{\mathrm{prime}}(m,n,\ell) \\
&\vdots \\
\rho_{\mathrm{sec},K}(m,n,\ell) &= g_{\mathrm{sec},K}(\ell) * z_{\mathrm{prime}}(m,n,\ell)
\end{aligned}\ , \tag{9}$$

where $g_{\mathrm{prime}}(\ell)$ is the primary homogenization filter and $g_{\mathrm{sec},k}(\ell)$ for $k = 1, 2, \ldots, K$ are the secondary homogenization filters. The primary filter $g_{\mathrm{prime}}(\ell)$ simply introduces a delay to maintain proper time alignment with the secondary responses and otherwise preserve primary filter response from (2). The structure of the secondary filters is arbitrary and chosen here to have discrete length C with uniform amplitude and containing random phase coefficients. Thus

$$\begin{aligned}
g_{\mathrm{prime}}(\ell) &= \delta\left(\ell - \frac{C}{2}\right) \\
g_{\mathrm{sec},k}(\ell) &= \frac{1}{\sqrt{C}} \exp\left(j 2\pi\, \theta_k(\ell)\right)
\end{aligned}\ , \tag{10}$$

where $\delta(\bullet)$ is the impulse function and each phase value is independently drawn from a uniform distribution on [−π, +π], where the random structure tends to provide filters with relatively low cross-correlation. The degree of range smearing provided by these random secondary filters is clearly dependent on length C and one could also design them to provide greater cross-correlation if desired.

To illustrate the utility of these secondary homogenization filters, consider a linear FM (LFM) waveform that has been pulse compressed with a normalized matched filter. Denote τ as the pulse duration and B as the swept bandwidth, with time-bandwidth product $B\tau$ specifying the dimensionality of the waveform and the number of samples needed to represent the discretised matched filter without over-sampling. In Figure 1, the pulse compressed response of an LFM waveform having $B\tau = 50$ is shown along with the responses from subsequent secondary filtering using lengths $C = B\tau$ and $C = 2B\tau$.

After primary matched filtering, the discrete pulse compression response for a point scatterer has duration $2B\tau - 1$. After the subsequent application of a secondary homogenization filter, this response extends to $2B\tau + C - 2$. As illustrated in Fig. 1, for $C = B\tau$, the primary response mainlobe gets smeared over half of the primary sidelobe interval. For $C = 2B\tau$, the primary mainlobe response gets smeared over the entire primary sidelobe interval, with commensurate reduction in average power as well. Therefore, as the homogenization filter length increases, the extent of mainlobe smearing increases, and the corresponding average power decreases.

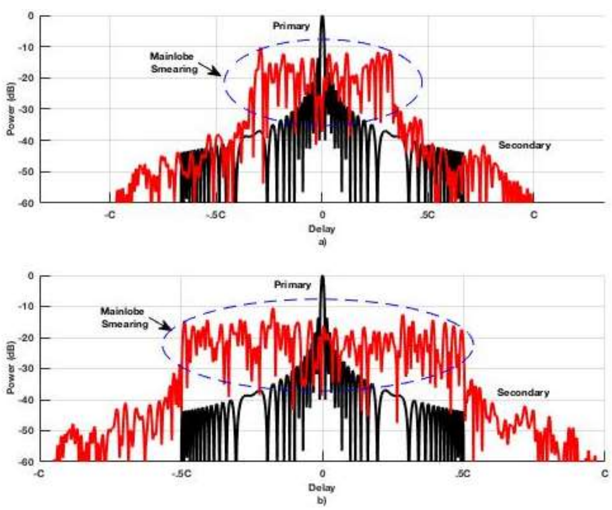

Figure 1: Mainlobe smearing for different homogenization filter lengths with $C = B\tau$ (top) and $C = 2B\tau$ (bottom)

Collecting the *MN* space-time samples for each range delay from the responses in (9) into the snapshot vectors $\boldsymbol{\rho}_{\text{prime}}(\ell)$, $\boldsymbol{\rho}_{\text{sec},1}(\ell)$, ..., $\boldsymbol{\rho}_{\text{sec},K}(\ell)$, SCM estimates similar to (6)-(8) can then be formed as

$$\hat{\mathbf{R}}_{\text{P}\mu,\text{prime}}(\ell_{\text{CUT}}) = \frac{1}{n(L_{\text{prime}})} \sum_{\substack{\ell \in L_{\text{prime}} \\ \ell \neq \ell_{\text{CUT}} \pm G}} \boldsymbol{\rho}_{\text{prime}}(\ell)\, \boldsymbol{\rho}_{\text{prime}}^{H}(\ell) \tag{11}$$

$$\hat{\mathbf{R}}_{\text{P}\mu,\text{NP}}(\ell_{\text{CUT}}) = \frac{1}{n(L_{\text{prime}})K} \sum_{k=1}^{K} \sum_{\ell \in L_{\text{prime}}} \boldsymbol{\rho}_{\text{sec},k}(\ell)\, \boldsymbol{\rho}_{\text{sec},k}^{H}(\ell) \tag{12}$$

and

$$\hat{\mathbf{R}}_{\text{P}\mu}(\ell_{\text{CUT}}) = \hat{\mathbf{R}}_{\text{P}\mu,\text{prime}}(\ell_{\text{CUT}}) + \hat{\mathbf{R}}_{\text{P}\mu,\text{NP}}(\ell_{\text{CUT}}), \tag{13}$$

respectively. As with the original μ-STAP formulation, these K additional channels of training data do not actually provide more independent sample support. While the smearing in range by these additional filters can make it appear that increased sample support is being obtained (when evaluating SINR for homogeneous clutter), this effect is really just a by-product of accessing a greater range extent than would otherwise be achieved by the single focused pulse compression filter (range sidelobes notwithstanding). To illustrate this distinction, in Section 5 we consider Pμ-STAP cases involving $K+1$ filters for $K=4$ according to (13) and the use of only 1 secondary filter without primary data via (11).

3. Analysis of Post μ-STAP Covariance Matrix

As with the original μ-STAP formulation of [30], it is not necessarily obvious that a good estimate of the interference covariance matrix is obtained for the CUT. Consequently, we follow a similar analysis as that performed in [30] to examine this covariance matrix under the condition of homogeneous clutter in noise.

The received signal model from (1) is first substituted into the first line of (2), yielding the primary pulse compression response

$$\begin{aligned} z_{\text{prime}}(m,n,t) &= h_{\text{prime}}(t) * y(m,n,t) \\ &= \sum_{\omega}\sum_{\theta}\left[\left(h_{\text{prime}}(t) * s(t)\right) * x(t,\omega,\theta,\theta_{\text{look}})\right] e^{j(m\omega+n\theta)} \\ &\quad + h_{\text{prime}}(t) * v(m,n,t) \\ &= \sum_{\omega}\sum_{\theta}\left[a(t) * x(t,\omega,\theta,\theta_{\text{look}})\right] e^{j(m\omega+n\theta)} \\ &\quad + \bar{v}(m,n,t) \end{aligned} \tag{14}$$

where $a(t) = h_{\text{prime}}(t) * s(t)$ is the standard matched (or mismatched) filter response that provides coherent integration gain and is generally desired to possess low sidelobes, and $\bar{v}(m,n,t)$ is the filtered noise. The pulse compression response in (14) is subsequently sampled, such that the fast-time variable t is replaced by the discrete range index ℓ. Note that, unlike in [30] where the prospect of different transmit spatial beampatterns is also considered, here we consider the emission of a single waveform and thus it is not necessary in this analysis to separate out the transmit beampattern from the scattering that it produces.

This discretised primary pulse compression response can then likewise be substituted into the set of the homogenisation filter responses of (9) such that

$$\begin{aligned}\rho_k(m,n,\ell) &= g_k(\ell) * z_{\text{prime}}(m,n,\ell) \\ &= \sum_{\omega}\sum_{\theta}\left[\left(g_k(\ell) * a(\ell)\right) * x(\ell,\omega,\theta,\theta_{\text{look}})\right]e^{j(m\omega+n\theta)} \\ &\quad + g_k(\ell) * \overline{v}(m,n,\ell) \\ &= \sum_{\omega}\sum_{\theta}\left[d_k(\ell) * x(\ell,\omega,\theta,\theta_{\text{look}})\right]e^{j(m\omega+n\theta)} \\ &\quad + \widehat{v}_k(m,n,\ell),\end{aligned} \tag{15}$$

in which $d_k(\ell) = g_k(\ell) * a(\ell)$ is the cross-correlation between the primary pulse compression response of the waveform and the kth homogenisation filter, and with $\widehat{v}_k(m,n,\ell)$ the (now twice) filtered noise. Note that we have indexed the primary homogenisation filter from (9) and (10) as $k = 0$ for simplicity. For the ℓth range index and kth homogenisation filter, the NM elements of (15) can be collected into the space-time response vector

$$\begin{aligned}\boldsymbol{\rho}_k(\ell) &= \sum_{\omega}\sum_{\theta}\left[d_k(\ell) * x(\ell,\omega,\theta,\theta_{\text{look}})\right]\mathbf{c}_{\text{st}}(\omega,\theta) \\ &\quad + \widehat{\mathbf{v}}_k(\ell).\end{aligned} \tag{16}$$

Based on the first line of (10) we observe that the $k = 0$ version of (16) is identical to the space-time snapshots used to form the standard SCM in (11). In contrast, the $k = 1, 2, \ldots, K$ versions of (16) are those used in (12) to form the Post μ-STAP SCM. In general, the SCM corresponding to the kth space-time response alone can be expressed as

$$\mathbf{R}_k(\ell) = E\left[\boldsymbol{\rho}_k(\ell)\ \boldsymbol{\rho}_k^H(\ell)\right], \tag{17}$$

into which (16) can be inserted, thereby yielding

$$\begin{aligned}&\mathbf{R}_k(\ell) \\ &= \sum_{\omega}\sum_{\theta}\left[\left|d_k(\ell)\right|^2 * E\left[\left|x(\ell,\omega,\theta,\theta_{\text{look}})\right|^2\right]\right] \\ &\quad \times \mathbf{c}_{\text{st}}(\omega,\theta)\ \mathbf{c}_{\text{st}}^H(\omega,\theta) + \mathbf{R}_{\hat{v},k}(\ell) \\ &= \sum_{\ell=-C}^{C}\left|d_k(\ell)\right|^2 \sum_{\omega}\sum_{\theta}\sigma_{\text{clut}}^2(\omega,\theta)\ \mathbf{c}_{\text{st}}(\omega,\theta)\ \mathbf{c}_{\text{st}}^H(\omega,\theta) \\ &\quad + \mathbf{R}_{\hat{v},k}(\ell).\end{aligned} \tag{18}$$

Here $\mathbf{R}_{\hat{v},k}(\ell)$ is the corresponding noise covariance and, like in [30], it has been assumed that every clutter patch is statistically independent. Thus $\sigma_{\text{clut}}^2(\omega,\theta)$ is the expected clutter power as a function of Doppler and spatial angle, which as noted above, subsumes the transmit spatial beampattern.

Given that the primary filtering in (10) is simply a delayed impulse, it is clear that the $k = 0$ version of (18) simplifies to the expectation of the primary SCM in (6), which is likewise the SISO form in [30]. Likewise, accounting for the transmit spatial beampattern being subsumed within the clutter response and the direct relationship between the summation over discretised cross-correlation terms in (18) and integration over a continuous cross-correlation response in [30, equation (29)], it can be readily surmised that (18) is an alternative form of the SIMO covariance matrix from [30], where Monte Carlo trials demonstrated that they retain the space-time characteristics of the primary covariance matrix.

4. Reduced-Dimension Multi-Waveform STAP

To avoid the repeated inversion of large SCMs, partially adaptive approaches have been developed [3, 34-36] that require less training data and incur a lower computational cost. As such, these implementations have become the standard means to actually realize STAP in practice.

Here, in addition to the full-dimension implementation, the Pμ-STAP scheme is evaluated in the context of well-known reduced-dimension implementations to assess the impact of their combination. Specifically, we examine element-space post-Doppler (ESPoD), beam-space pre-Doppler (BSPrD), and beam-space post-Doppler (BSPoD) formulations. The following summarizes these implementations and discusses how Pμ-STAP is incorporated into each.

4.1. Element-space post-Doppler Pμ-STAP

The multi-window element-space post-Doppler (ESPoD) implementation [34,35] applies different Doppler filters to the pulsed echoes received at each antenna element. In other words, for ESPoD the Doppler processing component is non-adaptive and localized to a set of D_t Doppler bins. Spatial processing is then fully adaptive across the N antenna elements. Therefore, each antenna element has an identical $M \times D_t$ filter bank $\mathbf{F}_m$ for the mth Doppler bin that is used to construct the $MN \times D_t N$ space-time transform

$$\mathbf{T}_m = \mathbf{F}_m \otimes \mathbf{I}_N\ . \tag{19}$$

There are different ways one can select the Doppler filters in (19). Here we consider the adjacent-bin approach [34], though pulse repetition interval (PRI) staggered [35] is likewise applicable in the Pμ-STAP context. Adjacent-bin post-Doppler employs the Doppler filters indexed by $m - P, \ldots, m, \ldots, m + P$ for

$$P = (D_t - 1)/2 . \quad (20)$$

Let $\mathbf{U} = [\mathbf{u}_0\ \mathbf{u}_1 \cdots \mathbf{u}_{M-1}]$ be an $M \times M$ discrete Fourier transform (DFT) matrix and $\mathbf{a}$ be an $M \times 1$ Doppler taper. The tapered mth Doppler filter is thus [3]

$$\mathbf{f}_m = \mathbf{a} \odot \mathbf{u}_m^* , \quad (21)$$

for $\odot$ the Hadamard product and $(\bullet)^*$ denoting complex conjugation, so that the mth Doppler filter bank is

$$\mathbf{F}_m = \left[\mathbf{f}_{m-P} \cdots \mathbf{f}_m \cdots \mathbf{f}_{m+P}\right] . \quad (22)$$

Note that D_t must be odd and the Doppler filter bank should wrap around the edges of the Doppler space [34].

In the same manner as reduced-dimension μ-STAP discussed in [33], the transform in (19) is applied to the Pμ-STAP training data of (9) as

$$\begin{aligned} \tilde{\boldsymbol{\rho}}_{\text{prime},m}(\ell) &= \mathbf{T}_m^H \boldsymbol{\rho}_{\text{prime}}(\ell) \\ \tilde{\boldsymbol{\rho}}_{\text{sec},1,m}(\ell) &= \mathbf{T}_m^H \boldsymbol{\rho}_{\text{sec},1}(\ell) \\ \tilde{\boldsymbol{\rho}}_{\text{sec},2,m}(\ell) &= \mathbf{T}_m^H \boldsymbol{\rho}_{\text{sec},2}(\ell) \\ &\vdots \\ \tilde{\boldsymbol{\rho}}_{\text{sec},K,m}(\ell) &= \mathbf{T}_m^H \boldsymbol{\rho}_{\text{sec},K}(\ell), \end{aligned} \quad (23)$$

thereby transforming the $MN \times 1$ primary and secondary snapshots into $D_t N \times 1$ snapshots. The space-time steering vector from (5) is likewise transformed as

$$\tilde{\mathbf{c}}_{\text{st},m}(\theta_{\text{look}}, \omega_{\text{D}}) = \mathbf{T}_m^H \mathbf{c}_{\text{st}}(\theta_{\text{look}}, \omega_{\text{D}}) . \quad (24)$$

Substituting (23) into (11)-(13) yields the ESPoD reduced-dimension SCM estimates

$$\tilde{\mathbf{R}}_{\text{P}\mu,\text{prime},m}(\ell_{\text{CUT}}) = \mathbf{T}_m^H \hat{\mathbf{R}}_{\text{P}\mu,\text{prime}}(\ell_{\text{CUT}}) \mathbf{T}_m \quad (25)$$

$$\tilde{\mathbf{R}}_{\text{P}\mu,\text{NP},m}(\ell_{\text{CUT}}) = \mathbf{T}_m^H \hat{\mathbf{R}}_{\text{P}\mu,\text{NP}}(\ell_{\text{CUT}}) \mathbf{T}_m , \quad (26)$$

and

$$\tilde{\mathbf{R}}_{\text{P}\mu,m}(\ell_{\text{CUT}}) = \mathbf{T}_m^H \hat{\mathbf{R}}_{\text{P}\mu}(\ell_{\text{CUT}}) \mathbf{T}_m, \quad (27)$$

respectively. The mth transformed filter is then obtained in the same manner as (4), yielding

$$\begin{aligned} \tilde{\mathbf{w}}_m(\ell_{\text{CUT}}, \theta_{\text{look}}, \omega_{\text{D}}) &= \tilde{\mathbf{R}}_m^{-1}(\ell_{\text{CUT}}) \tilde{\mathbf{c}}_{\text{st},m}(\theta_{\text{look}}, \omega_{\text{D}}) \\ &= \left(\mathbf{T}_m^H \hat{\mathbf{R}}(\ell_{\text{CUT}}) \mathbf{T}_m\right)^{-1} \mathbf{T}_m^H \mathbf{c}_{\text{st}}(\theta_{\text{look}}, \omega_{\text{D}}) \end{aligned} \quad (28)$$

for $\tilde{\mathbf{R}}_m$ and $\hat{\mathbf{R}}(\ell_{\text{CUT}})$ corresponding to one of the SCM estimates from (25)-(27), and response

$$\alpha_m(\ell_{\text{CUT}}, \omega_{\text{D}}) = \tilde{\mathbf{w}}_m^H(\ell_{\text{CUT}}, \theta_{\text{look}}, \omega_{\text{D}})\, \tilde{\boldsymbol{\rho}}_{\text{prime},m}(\ell_{\text{CUT}}) \quad (29)$$

when the filter is applied to the transformed primary data from (23). As discussed in [3], the actual filter response is then taken as the maximum value from (29) over index m.

The transformed adaptive filter can also be expressed in terms of the full MN-dimensional representation using the composite filter [3]

$$\begin{aligned} \mathbf{w}_m(\ell_{\text{CUT}}, \theta_{\text{look}}, \omega_{\text{D}}) &= \mathbf{T}_m \tilde{\mathbf{w}}_m(\ell_{\text{CUT}}, \theta_{\text{look}}, \omega_{\text{D}}) \\ &= \mathbf{T}_m \left(\mathbf{T}_m^H \hat{\mathbf{R}}(\ell_{\text{CUT}}) \mathbf{T}_m\right)^{-1} \mathbf{T}_m^H \mathbf{c}_{\text{st}}(\theta_{\text{look}}, \omega_{\text{D}}) \end{aligned} . \quad (30)$$

This composite filter perspective is used to facilitate the SINR analysis in Section 5.

4.2. Beam-space pre-Doppler Pμ-STAP

Beam-space pre-Doppler (BSPrD) techniques are related to displaced phase center antenna (DPCA) processing [36]. In contrast to element-space post-Doppler methods, in this formulation spatial beamforming is performed before adaptive processing, which may be performed over the full CPI, though the number of pulses M can be fairly large. It is therefore more efficient to reduce the MN-dimensional problem by beamforming over a subset of D_t pulses. Consequently, the CPI of M pulses is subdivided into a set of $\tilde{M}$ sub-CPIs consisting of D_t pulses each, where

$$\tilde{M} = M - D_t + 1 . \quad (31)$$

Each sub-CPI employs an identical bank of D_s beamformers for the nth antenna element, thereby realizing the $MN \times D_t D_s$ space-time transform

$$\mathbf{T}_{\tilde{m}n} = \mathbf{J}_{\tilde{m}} \otimes \mathbf{G}_n , \quad (32)$$

where $\mathbf{J}_{\tilde{m}}$ is the $M \times D_t$ selection matrix for the $\tilde{m}$th sub-CPI defined as

$$\mathbf{J}_{\tilde{m}} = \begin{bmatrix} \mathbf{0}_{\tilde{m} \times D_t} \\ \mathbf{I}_{D_t} \\ \mathbf{0}_{(M - D_t - \tilde{m}) \times D_t} \end{bmatrix} \quad (33)$$

and $\mathbf{G}_n$ is the nth beamformer matrix. The latter can be structured via displaced-beam or adjacent-beam [3, 36], which are spatial analogs to the PRI-staggered and adjacent-bin Doppler filter banks.

In like manner as before, we consider the adjacent-beam formulation, though Pμ-STAP may be used with either. Define the nth beamformer as [3]

$$\mathbf{g}_n = \mathbf{b} \odot \mathbf{u}_n^* , \quad (34)$$

where $\mathbf{b}$ is an $N \times 1$ spatial taper and $\mathbf{u}_n$ is the nth column of an $N \times N$ DFT matrix (based on the assumption of an ideal uniform linear array). The adjacent-beam formulation combines temporal samples from D_s spatial beams indexed as $n - Q$, …, n, …, $n +$

Q centered around the nth column of the DFT matrix, with $Q = (D_s - 1) / 2$.

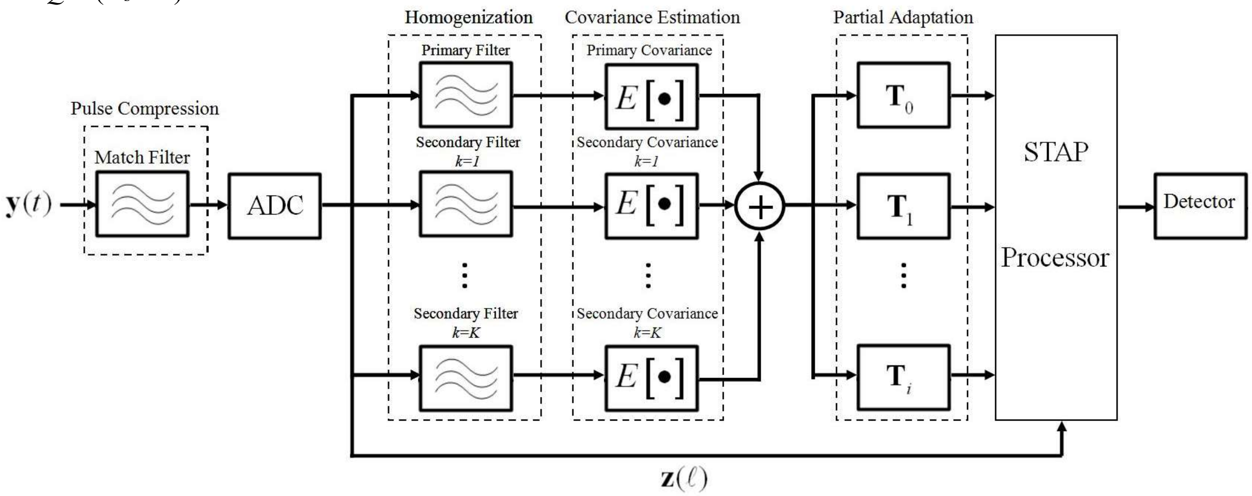

Figure 2: Receive Processing Chain for Partially Adaptive Post μ-STAP

The $N \times D_s$ reduced dimension beamforming matrix for the nth antenna element is thus

$$\mathbf{G}_n = \left[\mathbf{g}_{n-Q} \cdots \mathbf{g}_n \cdots \mathbf{g}_{n+Q} \right]. \tag{35}$$

Applying (32) to the discretized training data from (2) for μ-STAP or (9) for Pμ-STAP in the same manner as (23) realizes transformed primary and secondary snapshots of dimension $D_t D_s \times 1$. Likewise, the $D_t D_s \times D_t D_s$ reduced-dimension SCM estimates $\tilde{\mathbf{R}}_{\tilde{m},n}$ and an associated transformed space-time steering vector $\tilde{\mathbf{c}}_{\text{st},\tilde{m},n}(\theta_{\text{look}}, \omega_{\text{D}})$ can be obtained by applying the adjacent-beam transform (32) as in (25)-(27) and (24), respectively. Therefore, the nth adaptive beamformer for the $\tilde{m}$th sub-CPI is, like (28),

$$\begin{aligned}\tilde{\mathbf{w}}_{\tilde{m},n}(\ell_{\text{CUT}}, \theta_{\text{look}}, \omega_{\text{D}}) &= \tilde{\mathbf{R}}^{-1}_{\tilde{m},n}(\ell_{\text{CUT}}) \tilde{\mathbf{c}}_{\text{st},\tilde{m},n}(\theta_{\text{look}}, \omega_{\text{D}}) \\ &= \left(\mathbf{T}^H_{\tilde{m}n} \hat{\mathbf{R}}(\ell_{\text{CUT}}) \mathbf{T}_{\tilde{m}n}\right)^{-1} \mathbf{T}^H_{\tilde{m}n} \mathbf{c}_{\text{st}}(\theta_{\text{look}}, \omega_{\text{D}})\end{aligned} \tag{36}$$

for each particular combination of transformed primary/secondary data, with the corresponding full-dimension composite filter similar to (30) via

$$\begin{aligned}\mathbf{w}_{\tilde{m},n}(\ell_{CUT}, \theta_{\text{look}}, \omega_{\text{D}}) &= \mathbf{T}_{\tilde{m}n} \tilde{\mathbf{w}}_{\tilde{m},n}(\ell_{\text{CUT}}, \theta_{\text{look}}, \omega_{\text{D}}) \\ &= \mathbf{T}_{\tilde{m}n} \left(\mathbf{T}^H_{\tilde{m}n} \hat{\mathbf{R}}(\ell_{\text{CUT}}) \mathbf{T}_{\tilde{m}n}\right)^{-1} \mathbf{T}^H_{\tilde{m}n} \mathbf{c}_{\text{st}}(\theta_{\text{look}}, \omega_{\text{D}})\end{aligned}. \tag{37}$$

4.3. Beam-space post-Doppler μ-STAP

Finally, the beam-space post-Doppler (BSPoD) implementation pre-processes over both space and time by using the Doppler filter bank $\mathbf{F}_m$ from (22) as well as the beamformer matrix $\mathbf{G}_n$ from (35). This combined adjacent-bin/adjacent-beam formulation realizes the $MN \times D_t D_s$ space-time transform

$$\mathbf{T}_{mn} = \mathbf{F}_m \otimes \mathbf{G}_n, \tag{38}$$

which can be employed in the same manner as in (23)-(30) to transform the primary/secondary data, the space-time steering vector, the various SCM estimates, the reduced-dimension adaptive filter, and the full-dimension composite filter.

These space-time transforms and subsequent STAP implementations are all well known. Our purpose here is to consider them in the context of the Pμ-STAP scheme, which itself involves a transformation of the training data in the range domain, albeit for the purpose of enhanced robustness to non-homogeneous data instead of reducing dimensionality. Figure 2 illustrates a general diagram of the receive processing chain for reduced dimension Pμ-STAP. In the next section these various combinations are evaluated.

5. Assessment of Reduced-Dimension Pμ-STAP

SINR analysis is performed using a normalized SNR metric [4] cast in the partially adaptive framework. Using the optimum covariance $\mathbf{R}_{\text{opt}}$ based on clairvoyant knowledge and any composite filter via (30), the SINR for these reduced-dimension implementations can be stated as [3]

$$\text{SINR}(\omega_{\text{D}}) = \max_m \left\{ \frac{\left|\mathbf{w}^H_m \mathbf{c}_{\text{st}}\right|^2}{\mathbf{w}^H_m \mathbf{R}_{\text{opt}} \mathbf{w}_m} \right\}, \tag{39}$$

where the dependencies on ℓ_{CUT}, θ_{look}, and ω_{D} in $\mathbf{w}_m$ have been suppressed for brevity. By setting $\hat{\mathbf{R}}(\ell_{\text{CUT}}) = \mathbf{R}_{\text{opt}}$ within the determination of $\mathbf{w}_m$, (39) becomes the fully adaptive clairvoyant SINR defined as

$$\mathrm{SINR}_{\mathrm{opt}}(\omega_{\mathrm{D}}) = \mathbf{c}_{\mathrm{st}}^{H}\mathbf{R}_{\mathrm{opt}}^{-1}\mathbf{c}_{\mathrm{st}}\,. \tag{40}$$

Normalizing the SINR from (39) by SNR also yields the SINR loss factor [4]

$$L_{\mathrm{SINR}}(\omega_{\mathrm{D}}) = \frac{\mathrm{SINR}(\omega_{\mathrm{D}})}{\mathrm{SNR}} \tag{41}$$

that compares interference-limited performance to noise-limited performance, here also including the impact of the given covariance matrix estimate and the dimensionality reducing transform.

Let $f_{\min} = \omega_{\min} / 2\pi$ be the clairvoyant minimum detectable Doppler (MDD) from [3], defined as

$$f_{\min}(L_{\mathrm{SINR}}) = \frac{1}{2}\left(f_{\mathrm{U}}(L_{\mathrm{SINR}}) - f_{\mathrm{L}}(L_{\mathrm{SINR}})\right), \tag{42}$$

where $f_{\mathrm{L}}(L_{\mathrm{SINR}})$ and $f_{\mathrm{U}}(L_{\mathrm{SINR}})$ demarcate the lower and upper Doppler edge frequencies of the clutter notch, respectively. The minimum detectable velocity can then be obtained by multiplying $f_{\min}$ by a half-wavelength. We consider the clutter notch edges to be the frequencies at which $L_{\mathrm{SINR}}(\omega_{\mathrm{D}})$ from (41) equals −3dB. For the parameters used in these simulations and based on clairvoyant knowledge of the clutter, the normalized clairvoyant MDD is $f_{\min}(L_{\mathrm{SINR}}) \cong 0.13$, which as observed in Fig. 3 could be positive or negative.

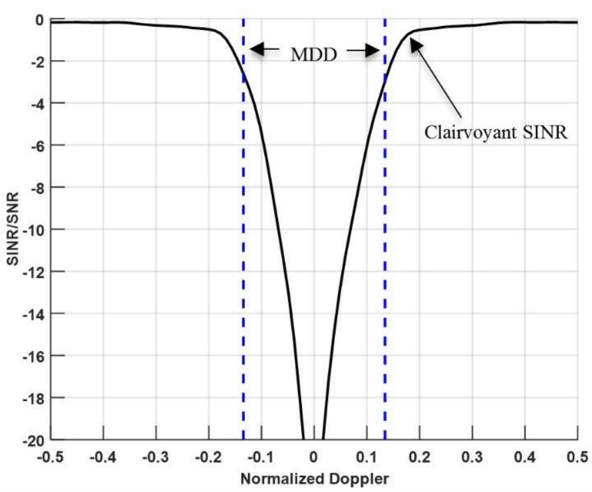

Figure 3: Clairvoyant Minimum Detectable Doppler

It is also useful to define an estimation loss factor [4, 30] that relates SINR performance for an estimated SCM via (39) to the SINR performance based on the optimal (clairvoyant) covariance knowledge. In contrast to the worst-case loss factor defined in [30], here we consider the average loss defined as

$$\underset{\omega_{\mathrm{D}}}{\mathrm{mean}}\left\{\frac{\mathrm{SINR}(\omega_{\mathrm{D}})}{\mathrm{SINR}_{\mathrm{opt}}(\omega_{\mathrm{D}})}\right\} \tag{43}$$

which is computed over $\omega_{\mathrm{D}} < -\omega_{\min}$ and $\omega_{\mathrm{D}} > +\omega_{\min}$ (i.e. outside the clutter notch region). This value is determined as a function of the number of range sample intervals included in SCM estimation for different implementation schemes and clutter scenarios.

5.1. Simulation parameters

Consider an airborne multichannel GMTI radar that is side-looking. Here the antenna is an $N = 11$ element uniform linear array with half-wavelength spacing that emits a CPI of $M = 21$ identical pulsed waveforms. The platform is assumed to have no crab angle and traverses one half-interelement spacing during the CPI (so $\beta = 1$). The clutter is generated by dividing the range ring in azimuth into 241 ($> NM = 231$) equal-sized clutter patches. The scattering from each patch is IID, drawn from a complex Gaussian distribution, and scaled such that the total clutter-to-noise ratio (CNR) is 54 dB. The thermal noise is also complex white Gaussian.

For beam-space dimensionality reduction the $N = 11$ receive elements are reduced to $D_{\mathrm{s}} = 5$ beams. The post-Doppler implementations likewise reduce the $M = 21$ pulses in the CPI to either $D_{\mathrm{t1}} = 5$ or $D_{\mathrm{t2}} = 11$ pulses in each sub-CPI to assess different sample support regimes. The adjacent-bin and adjacent-beam implementations are both uniformly tapered.

The number of range samples used to estimate the SCM is varied from 1 to $2NM = 462$. For Pμ-STAP, the number of range samples for SCM estimation is varied from $(K+1)$ to $(K+1)2NM$ due to the additional training data provided by the K secondary filters. Diagonal loading is employed for all SCM estimates using the true noise power. The primary (transmit) waveform used here is an optimized polyphase-coded FM (PCFM) waveform [39, 40] that has a time-bandwidth product of $BT = 100$. Generation of this waveform is outlined in Appendix A of [30]. Four secondary homogenization filters ($K = 4$) are used via (9) to provide no more than 17 dB of normalized cross-correlation with the primary waveform. Figure 4 shows the particular primary and secondary filter responses, with the primary (delayed matched filter) response in black realizing a peak sidelobe level of nearly −44 dB.

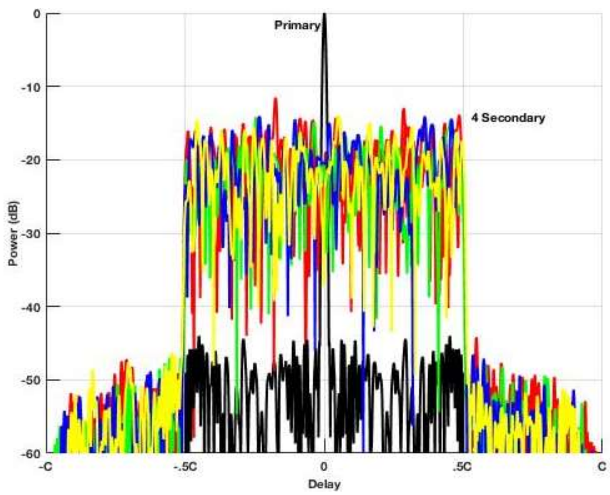

Figure 4: Primary and secondary filter responses to an optimized PCFM waveform

Performance of reduced-dimension Pμ-STAP is evaluated for three environments: 1) non-homogeneous clutter, 2) non-homogeneous clutter with a large discrete in the CUT, and 3) non-homogeneous clutter with several modest targets in the training data. The SINR loss for each clutter scenario and dimensionality reduction combination is averaged over 50 independent Monte Carlo trials.

We present a comparison between the standard (primary only) STAP SCM and two Pμ-STAP formulations: *a*) primary plus 4 secondary filters, and *b*) only 1 secondary filter. Each of these is implemented according to fully adaptive and partially adaptive formulations. Table I shows the different receive processing configurations.

Table 1 Receive processing configurations

Receive Processing	Line style/color
primary only, full ($M = 21$)	solid blue
primary only, partial ($D_{t1} = 5$)	solid red
primary only, partial ($D_{t2} = 11$)	solid green
secondary only ($K = 1$), full ($M = 21$)	dotted blue
secondary only ($K = 1$), partial ($D_{t1} = 5$)	dotted red
secondary only ($K = 1$), partial ($D_{t2} = 11$)	dotted green
primary & $K = 4$ sec., full ($M = 21$)	dashed blue
primary & $K = 4$ sec., partial ($D_{t1} = 5$)	dashed red
primary & $K = 4$ sec., partial ($D_{t2} = 11$)	dashed green

5.2. Non-homogeneous clutter

Like in [30], non-homogeneous clutter is modeled by randomly modulating the power of each complex Gaussian range/angle clutter patch using a Weibull distribution with a shape parameter of 1.7 [37, 38]. To accompany this local modulation, an exponentially distributed regional clutter modulation with $\lambda = 0.05$ is applied independently to each region (here 10 range cells × $1/N$ angle segments). Random internal clutter motion (ICM) is also introduced that is uniformly distributed on ±2% relative to the normalized Doppler response. These values were selected because they were found to produce noticeable degradation for standard STAP but they are otherwise arbitrary.

For the adjacent-bin implementation of element-space post-Doppler (ESPoD) Pμ-STAP from Section 4.1, Fig. 5 shows the SINR estimation loss factor of (43) as a function of training data sample support. As the number of sub-CPIs are reduced from $D_{t2} = 11$ to $D_{t1} = 5$, modest improvement is observed due to the need for less training data. It is also observed that Pμ-STAP using primary + 4 secondary sets of training data realizes an enhancement similar to that observed for the original μ-STAP approach in [30]. When this arrangement is combined with the $D_{t1} = 5$ partially adaptive implementation the best performance is realized, particularly at very low sample support.

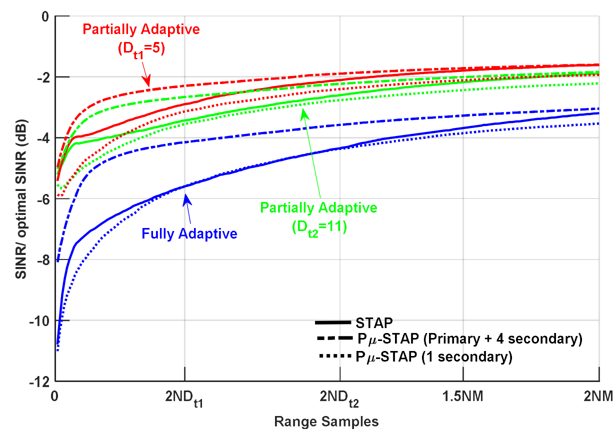

Figure 5: SINR estimation loss from (43) versus sample support using ESPoD in non-homogeneous clutter

Table 2 SINR estimation loss via (43) per sample support for non-homogeneous clutter using ESPoD (in dB)

Receive Processing	$2ND_{t1}$	$2ND_{t2}$
primary only, full ($M = 21$)	−5.60	−4.34
primary only, partial ($D_{t1} = 5$)	−2.90	−2.10
primary only, partial ($D_{t2} = 11$)	−3.43	−2.60
secondary only, full ($M = 21$)	−5.59	−4.36
secondary only, partial ($D_{t1} = 5$)	−3.14	−2.40
secondary only, partial ($D_{t2} = 11$)	−3.55	−2.76
primary + 4 sec., full ($M = 21$)	−4.15	−3.58
primary + 4 sec., partial ($D_{t1} = 5$)	−2.30	−1.89
primary + 4 sec., partial ($D_{t2} = 11$)	−2.66	−2.23

Table 2 presents values of the estimation loss factor from (43) for $2ND_{t1}$ and $2ND_{t2}$ range sample intervals used as training data. Because the reduced dimension schemes inherently require lower sample support, there is less SINR loss than is encountered for the fully adaptive cases, particularly at these lower sample values that may be necessary for highly non-homogeneous clutter environments.

In particular, the highlighted values illustrate the achieved SINR loss corresponding to the RMB rule for sample support (i.e. twice the degrees of freedom) [1, 2]. When a single set of Pμ-STAP secondary training data (middle three rows in Table 2) is used in place of the primary (matched filtered) training data (top three rows), a small degradation is incurred. However, this result does show the general utility of the secondary data that is obtained by the use of a homogenization filter per (23). Moreover, when four sets of secondary data are combined with the primary training data – noting that these data sets involve different range domain mixtures of <u>the same</u> received clutter response – an SINR improvement of roughly 0.2 dB (for $2ND_{t1}$ samples) and 0.8 dB (for $2ND_{t2}$ samples) is realized for this scenario due to the beneficial range smearing of non-homogeneous clutter.

In Fig. 6, the SNR-normalized SINR from (41) is plotted relative to normalized Doppler for $2ND_{t1}$ range sample intervals of training data (last column in Table 2). Here it is observed that the minimum detectable velocity (MDV via direct extension of MDD) is likewise improved for partially adaptive Pμ-STAP compared to the standard (primary only) partially adaptive STAP implementation. Similar plots for the BSPrD and BSPoD implementations are excluded since the results are comparable to that observed in Fig. 6 for ESPoD.

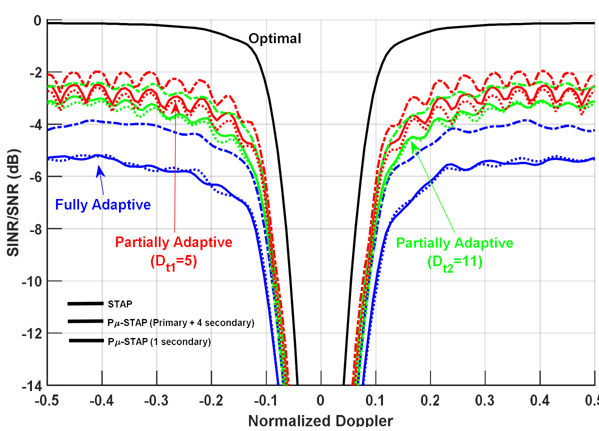

Figure 6: SNR-normalized SINR from (41) versus normalized Doppler using ESPoD in non-homogeneous clutter for $2ND_{t1}$ training data sample intervals

In Fig. 7, the SINR loss via (43) for the beam-space pre-Doppler (BSPrD) implementation of Section 4.2 is shown when reducing from $N = 11$ elements to $D_s = 5$ beams and from $M = 21$ pulses to $D_{t1} = 5$ or $D_{t2} = 11$ pulses in each sub-CPI. While the differences are less distinct as for the ESPoD arrangement, the SINR enhancement afforded by the Pμ-STAP version is still evident, particularly at low sample support.

Table 3 likewise illustrates the SINR loss for the BSPrD implementation of these different SCM estimators at sample support values of $2D_sD_{t1}$ and $2D_sD_{t2}$. As in the previous ESPoD case, the combination of the reduced dimension implementation and multiple sets of Pμ-STAP training data provides the best performance.

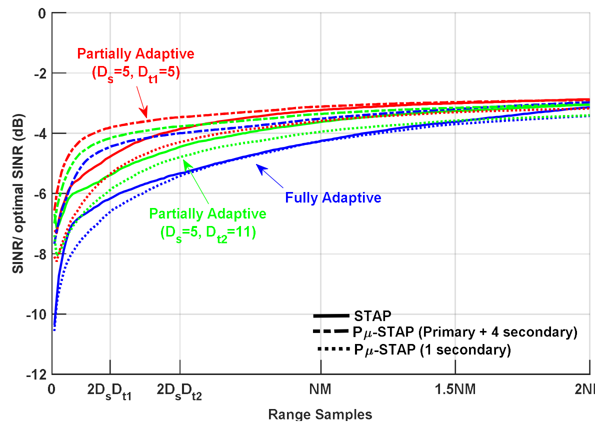

Figure 7: SINR estimation loss from (43) versus sample support using BSPrD in non-homogeneous clutter

Table 3 SINR estimation loss via (43) per sample support for non-homogeneous clutter using BSPrD (in dB)

Receive Processing	$2D_sD_{t1}$	$2D_sD_{t2}$
primary only, full ($M = 21$)	−6.17	−5.33
primary only, partial ($D_{t1} = 5$)	−4.77	−3.86
primary only, partial ($D_{t2} = 11$)	−5.39	−4.45
secondary only, full ($M = 21$)	−6.61	−5.41
secondary only, partial ($D_{t1} = 5$)	−5.35	−4.29
secondary only, partial ($D_{t2} = 11$)	−5.88	−4.79
primary + 4 sec., full ($M = 21$)	−4.45	−4.00
primary + 4 sec., partial ($D_{t1} = 5$)	−3.81	−3.47
primary + 4 sec., partial ($D_{t2} = 11$)	−4.16	−3.77

Finally, Fig. 8 shows the SINR loss of (43) for the beam-space post-Doppler (BSPoD) implementation of Section 3.3, which also uses $D_s = 5$ beams and $D_{t1} = 5$ or $D_{t2} = 11$ pulses in each sub-CPI. Like ESPoD, this scheme realizes significant SINR improvement compared to the fully adaptive implementations. While relatively modest in this case, further enhancement is still observed when using multiple sets of Pμ-STAP training data. In short, all three of these reduced dimension schemes work well with Pμ-STAP for non-homogeneous clutter and their combination provides enhanced SINR at low sample support.

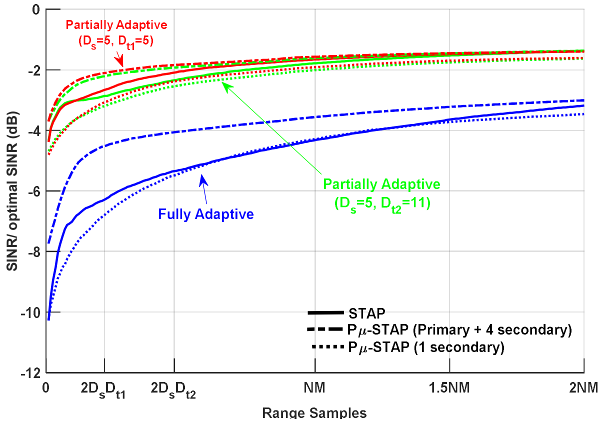

Figure 8: SINR estimation loss from (43) versus sample support using BSPoD in non-homogeneous clutter

5.3. Clutter Discrete in CUT

The presence of a clutter discrete in the cell under test (CUT) is a form of non-homogeneous interference that degrades SINR because the space-time structure of the training data differs from that in the CUT. Further, clutter discretes can also be erroneously detected as actual moving targets. Here we consider a clutter scenario in which a large discrete (20 dB above the average clutter power) is present in the CUT and the rest of the clutter is non-homogeneous in the same manner as the previous section. While such a large discrete would likely be detected as an outlier and subsequently excised prior to the application of STAP, the point here is to illustrate the capability of Pμ-STAP to compensate for discretes that are not excised, such as may occur in complex environments.

For the ESPoD reduced dimension implementation, Fig. 9 depicts the SINR estimation loss of (43) and Table 4 presents specific loss values for different processing arrangements using $2ND_{t1}$ and $2ND_{t2}$ range sample intervals as training data. Compared to the discrete-free (but otherwise still non-homogeneous clutter) results from Fig. 5 and Table 2, the large discrete imposes of a 1-2 dB further SINR loss depending on the particular implementation. Specifically, for $D_{t1} = 5$ pulses in each sub-CPI and $2ND_{t1}$ range sample intervals, the primary-only and secondary-only cases experience 1.11 and 0.98 dB of additional SINR loss while the "primary + 4 secondary" Pμ-STAP scheme realizes 0.84 dB of further loss. It is also rather clear in Fig. 9 that the Pμ-STAP traces corresponding to the "primary + 4 secondary" cases in are superior to the other training data schemes.

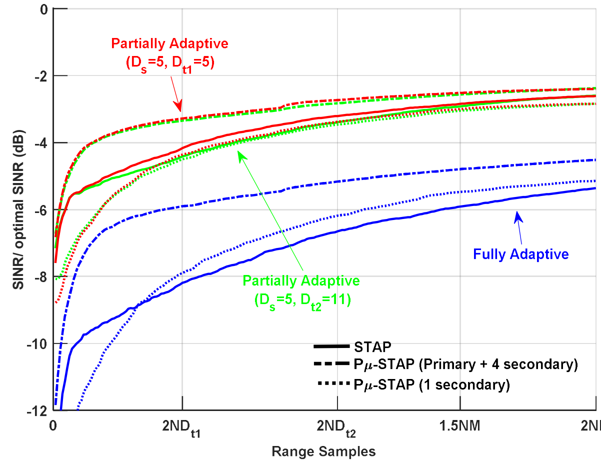

Figure 9: SINR estimation loss from (43) versus sample support using ESPoD in non-homogeneous clutter with a discrete in the CUT

Table 4 SINR estimation loss via (43) per sample support for non-homogeneous clutter and discrete in the CUT using ESPoD (in dB)

Receive Processing	$2ND_{t1}$	$2ND_{t2}$
primary only, full ($M = 21$)	−6.65	−8.18
primary only, partial ($D_{t1} = 5$)	−3.21	−4.17
primary only, partial ($D_{t2} = 11$)	−3.39	−4.41
secondary only, full ($M = 21$)	−6.18	−7.89
secondary only, partial ($D_{t1} = 5$)	−3.38	−4.36
secondary only, partial ($D_{t2} = 11$)	−3.46	−4.50
primary + 4 sec., full ($M = 21$)	−5.17	−5.90
primary + 4 sec., partial ($D_{t1} = 5$)	−2.73	−3.28
primary + 4 sec., partial ($D_{t2} = 11$)	−2.83	−3.34

Figures 10 and 11 likewise illustrate the SINR estimation loss of (43) for this clutter discrete scenario when using the BSPrD and BSPoD reduced dimension implementations. While the latter reveals the least difference between standard (primary only) and Pμ-STAP SCM estimation, both of these reduced dimension implementations show that the "primary + 4 secondary" Pμ-STAP versions again provide an SINR performance enhancement benefit.

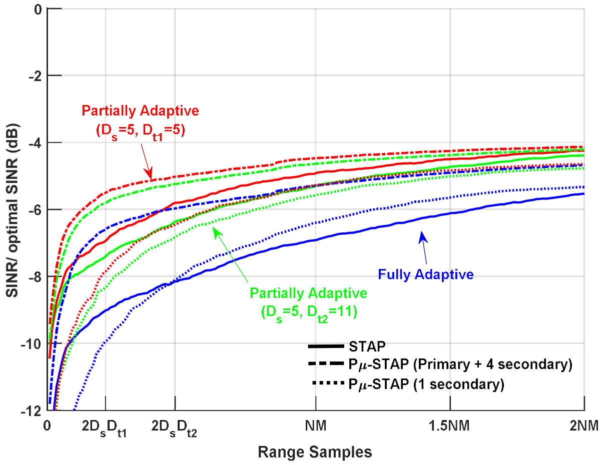

Figure 10: SINR estimation loss from (43) versus sample support using BSPrD in non-homogeneous clutter with a discrete in the CUT

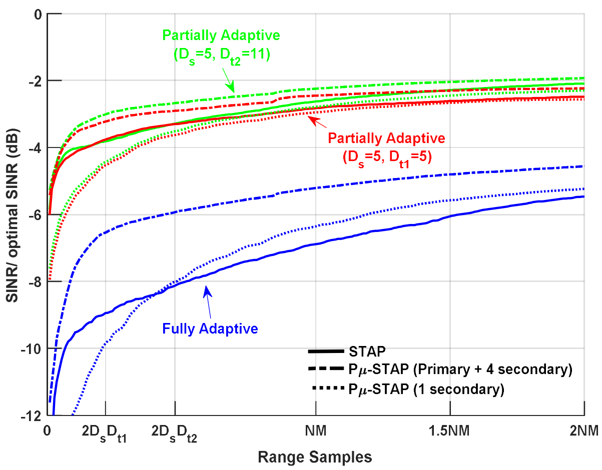

Figure 11: SINR estimation loss from (43) versus sample support using BSPoD in non-homogeneous clutter with a discrete in the CUT

Table 5 provides specific loss values of the BSPrD implementations for different processing arrangements using $2ND_{t1}$ and $2ND_{t2}$ range sample intervals as training data. In the same manner as with ESPoD, for $D_{t1} = 5$ pulses and $2ND_{t1}$ range sample intervals the BSPrD implementation for the clutter discrete scenario compared to the discrete-free scenario (Table 3) experiences 2.18, 2.52, and 1.70 dB of additional SINR loss for the primary-only, secondary-only, and "primary + 4 secondary" training data schemes. These results again illustrate the improved robustness provided by Pμ-STAP for reduced dimension implementations.

Table 5 SINR estimation loss via (43) per sample support for non-homogeneous clutter and discrete in the CUT using BSPrD (in dB)

Receive Processing	$2ND_{t1}$	$2ND_{t2}$
primary only, full ($M = 21$)	−9.02	−8.16
primary only, partial ($D_{t1} = 5$)	−7.40	−6.36
primary only, partial ($D_{t2} = 11$)	−6.95	−5.80
secondary only, full ($M = 21$)	−9.95	−8.10
secondary only, partial ($D_{t1} = 5$)	−8.35	−6.82
secondary only, partial ($D_{t2} = 11$)	−7.87	−6.45
primary + 4 sec., full ($M = 21$)	−6.60	−5.97
primary + 4 sec., partial ($D_{t1} = 5$)	−5.81	−5.24
primary + 4 sec., partial ($D_{t2} = 11$)	−5.51	−5.02

Finally, Fig. 12 shows the SNR-normalized SINR from (41) plotted relative to normalized Doppler for $2D_sD_{t1}$ range sample intervals of training data for the BSPoD implementation when a large clutter discrete is present. The important take-away from this figure is that the different realizations of Pμ-STAP using "primary + 4 secondary" all provide some MDV enhancement, though with diminishing improvement as the dimensionality is further reduced.

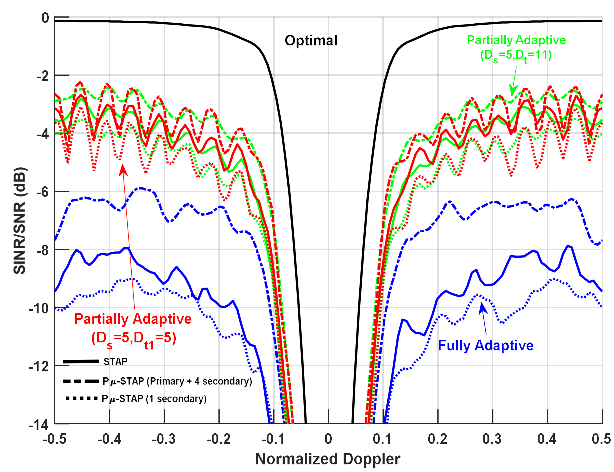

Figure 12: SNR-normalized SINR from (41) versus normalized Doppler using BSPoD in non-homogeneous clutter and discrete in the CUT for $2D_sD_{t1}$ training data sample intervals

5.4. Targets in Training Data

The last non-homogeneous effect we consider involves the presence of targets in the training data that are known to contaminate the SCM in such a way that can ultimately lead to substantial SINR loss for a prospective target in the CUT. In this context the benefit of Pμ-STAP is that, since such targets would tend to be relatively few in number compared to the pervasive and higher power clutter response, the range smearing effect should drive the target contributions to a level near or even below the noise floor on a per-range-cell basis.

Consequently, their contribution to the SCM would be greatly reduced, thereby at least partly ameliorating the SINR loss that otherwise occurs.

Here we consider ten targets that reside in the range cells surrounding the CUT (beyond the guard cells) that have 15 dB SNR, normalized Doppler of 0.5, and scattering phase that is otherwise random and independent. Because they possess rather modest SNR and are grouped together, such a target arrangement could be difficult to address via pre-processing based on non-homogeneity detection, yet their combination could be rather detrimental to SINR since they have the same Doppler.

Figures 13-15 show the SNR-normalized SINR from (41) for the ESPoD, BSPrD, and BSPoD implementations, respectively. Of particular note is the loss incurred at the 0.5 normalized Doppler where the 10 targets reside. However, it is observed that the "primary + 4 secondary" Pμ-STAP SCM estimates do provide greater robustness in the form of less severe SINR loss by virtue of the range smearing effect of the secondary training data sets. Moreover, the reduced dimension versions of Pμ-STAP reveal ever greater robustness, with the partially adaptive BSPoD implementation in Fig. 15 showing almost no degradation at all.

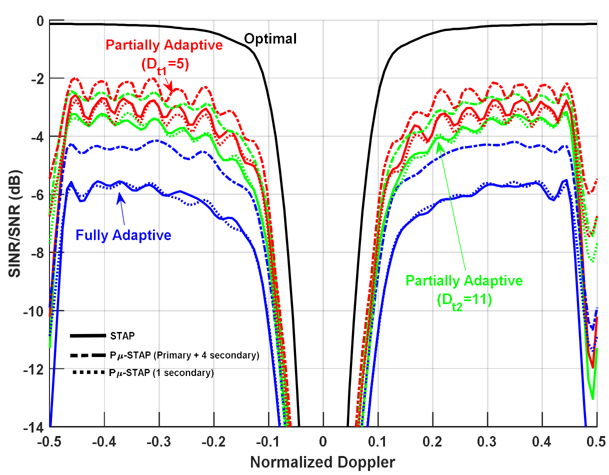

Figure 13: SNR-normalized SINR from (41) versus normalized Doppler using ESPoD in non-homogeneous clutter and 10 targets in the training data for $2ND_{t1}$ training data sample intervals

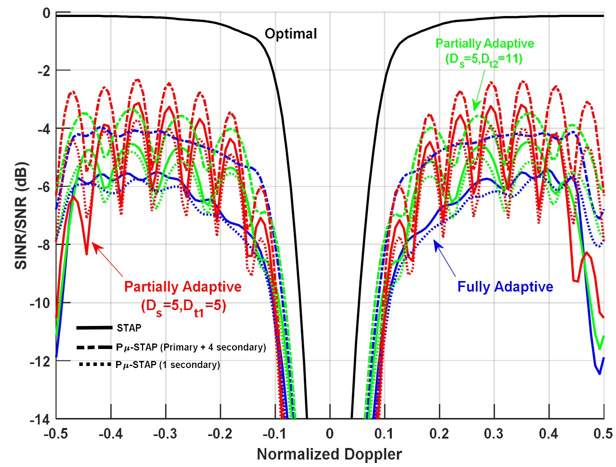

Figure 14: SNR-normalized SINR from (41) versus normalized Doppler using BSPrD in non-homogeneous clutter and 10 targets in the training data for $2D_sD_{t1}$ training data sample intervals

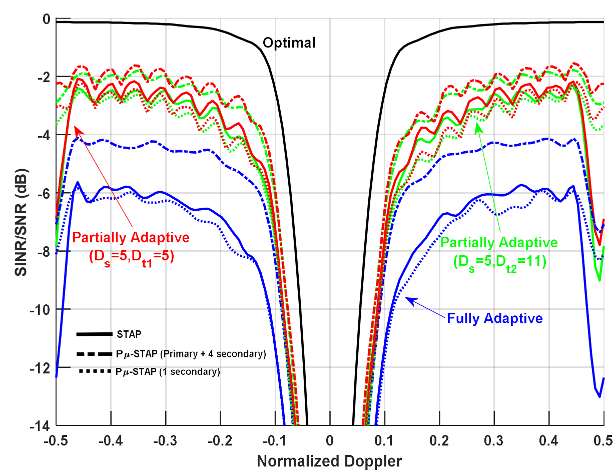

Figure 15: SNR-normalized SINR from (41) versus normalized Doppler using BSPoD in non-homogeneous clutter and 10 targets in the training data for $2D_sD_{t1}$ training data sample intervals

6. Conclusions

A new post-processing form of multi-waveform space-time adaptive processing (μ-STAP) denoted as post μ-STAP (or Pμ-STAP) was introduced and combined with well known partially adaptive STAP implementations to assess the prospective robustness enhancements that could be achieved in practice. For simulated clutter it has been observed that Pμ-STAP outperforms STAP under several non-homogeneous scenarios including a discrete in the CUT and multiple similar targets of modest size in the training data. Further, the combination of Pμ-STAP with reduced dimension implementations realizes very good SINR performance with rather low training data sample support.

7. References

[1] L.E. Brennan, I.S. Reed, "Theory of adaptive radar," *IEEE Trans. Aerospace & Electronic Systems*, vol. AES-9, no. 2, pp. 237-252, Mar. 1973.

[2] I.S. Reed, J.D. Mallett, L.E. Brennan, "Rapid convergence rate in adaptive arrays," *IEEE Trans. Aerospace & Electronic Systems*, vol. AES-10, no. 6, pp. 853-863, Nov. 1974.

[3] J. Ward, "Space-time adaptive processing for airborne radar," *Lincoln Lab Tech. Report*, TR-1015, Dec. 1994.

[4] W.L. Melvin, "A STAP overview," *IEEE Aerospace & Electronic Systems Mag.*, vol. 19, no.1, pp.19-35, Jan. 2004.

[5] W.L. Melvin, "Space-time adaptive radar performance in heterogeneous clutter," *IEEE Trans. Aerospace & Electronic Systems*, vol. 36, no. 2, pp. 621-633, Apr. 2000.

[6] E.C. Barile, R.L. Fante, J.A. Torres, "Some limitations on the effectiveness of airborne adaptive radar," *IEEE Trans. Aerospace & Electronic Systems*, vol. 28, no. 4, pp. 1015-1032, Oct. 1992.

[7] J.R. Guerci, "Theory and application of covariance matrix tapers for robust adaptive beamforming," *IEEE Trans. Signal Processing*, vol. 47, no. 4, pp. 977-985, Apr. 1999.

[8] D.J. Rabideau, A.O. Steinhardt, "Improved adaptive clutter cancellation through data-adaptive training," in *IEEE Transactions on Aerospace and Electronic Systems*, vol. 35, no. 3, pp. 879-891, Jul 1999.

[9] S.M. Kogon, M.A. Zatman, "STAP adaptive weight training using phase and power selection criteria," *35th Asilomar Conf. Signals, Systems and Computers*, Pacific Grove, CA, USA, Nov. 2001.

[10] G. Benitz, J. D. Griesbach, C. Rader, "Two-parameter power-variable-training STAP," *38th Asilomar Conf. Signals, Systems and Computers*, Nov. 2004.

[11] T.M. Selee, K.F. Bing, W.L. Melvin, "STAP application in mountainous terrain: Challenges and strategies," *IEEE Radar Conf.*, Atlanta, GA, USA, May 2012.

[12] J.R. Roman, M. Rangaswamy, D.W. Davis, Q. Zhang, B. Himed, J.H. Michels,"Parametric adaptive matched filter for airborne radar applications," *IEEE Trans. Aerospace & Electronic Systems*, vol. 36, no. 2, pp. 677-692, Apr. 2000.

[13] R.S. Adve, T.B. Hale, M.C. Wicks, "Practical joint domain localized adaptive processing in homogeneous and nonhomogeneous environments. Part 2: nonhomogeneous environments," *IEE Proc. Radar, Sonar & Navigation*, vol. 147, no. 2, pp. 66-74, Apr. 2000.

[14] T.K. Sarkar, H. Wang, S. Park, R. Adve, J. Koh, K. Kim, Y. Zhang, M.C. Wicks, R.D. Brown, "A deterministic least-squares approach to space-time adaptive processing (STAP)," *IEEE Trans. Antennas & Propagation*, vol. 49, no. 1, pp. 91-103, Jan. 2001.

[15] G.A. Fabrizio, M.D. Turley, "An advanced STAP implementation for surveillance radar systems," *IEEE Workshop on Statistical Signal Processing*, Singapore, pp. 134-137, 6-8 Aug. 2001.

[16] K. Gerlach, "Outlier resistance adaptive matched filtering," *IEEE Trans. Aerospace & Electronic Systems*, vol. 38, no. 3, pp. 885-901, July 2002.

[17] K. Gerlach, M.L. Picciolo, "Airborne/spacebased radar STAP using a structured covariance matrix," *IEEE Trans. Aerospace & Electronic Systems*, vol. 39, no. 1, pp. 269-281, Jan. 2003.

[18] Y.-L. Wang, J.-W. Chen, Z. Bao, Y.-N. Peng, "Robust space-time adaptive processing for airborne radar in nonhomogeneous environments," *IEEE Trans. Aerospace & Electronic Systems*, vol. 39, no. 1, pp. 70-81, Jan. 2003.

[19] M.L. Picciolo, K. Gerlach, "Median cascaded canceller for robust adaptive array processing," *IEEE Trans. Aerospace & Electronic Systems*, vol. 39, no. 3, pp. 883-900, July 2003.

[20] K. Gerlach, S.D. Blunt, M.L. Picciolo, "Robust adaptive matched filtering using the FRACTA algorithm," *IEEE Trans. Aerospace & Electronic Systems*, vol. 40, no. 3, pp. 929-945, July 2004.

[21] S.D. Blunt, K. Gerlach, "Efficient robust AMF using the FRACTA algorithm," *IEEE Trans. Aerospace & Electronic Systems*, vol. 41, no. 2, pp. 537-548, Apr. 2005.

[22] W.L. Melvin, J.R. Guerci, "Knowledge-aided signal processing: a new paradigm for radar and other advanced sensors," *IEEE Trans. Aerospace & Electronic Systems*, vol. 42, no. 3, pp. 983-996, July 2006.

[23] W.L. Melvin, G.A. Showman, "An approach to knowledge-aided covariance estimation," *IEEE Trans. Aerospace & Electronic Systems*, vol. 42, no. 3, pp. 1021-1042, July 2006.

[24] S.D. Blunt, K. Gerlach, M. Rangaswamy, "STAP using knowledge-aided covariance estimation and the FRACTA algorithm," *IEEE Trans. Aerospace & Electronic Systems*, vol. 42, no. 3, pp. 1043-1057, July 2006.

[25] F. Gini, M. Rangaswamy, eds., *Knowledge Based Radar Detection, Tracking, and Classification*, John Wiley & Sons, Inc., 2008.

[26] E. Aboutanios, B. Mulgrew, "Hybrid detection approach for STAP in heterogeneous clutter," *IEEE Trans. Aerospace & Electronic Systems*, vol. 46, no. 3, pp. 1021-1033, July 2010.

[27] O. Besson, S. Bidon, "Adaptive processing with signal contaminated training samples," *IEEE Trans. Signal Processing*, vol. 61, no. 17, pp. 4318-4329, Sept. 2013.

[28] S.D. Blunt, J. Jakabosky, J. Metcalf, J. Stiles, and B. Himed, " Multi-waveform STAP," *IEEE Radar Conf.*, Ottawa, Canada, Apr./May 2013.

[29] S.D. Blunt, J. Metcalf, J. Jakabosky, and B. Himed, "SINR analysis of multi-waveform STAP," *International Radar Conf.*, Lille, France, Oct. 2014.

[30] S.D. Blunt, J. Metcalf, J. Jakabosky, J. Stiles, B. Himed, "Multi-waveform space-time adaptive processing," *IEEE Trans. Aerospace & Electronic Systems*, vol. 53, no. 1, pp. 385-404, Feb. 2017.

[31] D.M. Boroson, "Sample size considerations for adaptive arrays," *IEEE Trans. Aerospace & Electronic Systems*, vol. AES-16, no. 4, pp. 446-451, July 1980.

[32] K. Gerlach, "The effects of signal contamination on two adaptive detectors," *IEEE Trans. Aerospace & Electronic Systems*, vol. 31, no. 1, pp. 297-309, Jan. 1995.

[33] L. Harnett, P.M. McCormick, S.D. Blunt, J.G. Metcalf, "Multi-window post-Doppler dimensionality reduction for multi-waveform STAP," *IEEE Radar Conf.*, Philadelphia, PA, USA, May 2016.

[34] R.C. DiPietro, "Extended factored space-time processing for airborne radar systems," *26th Asilomar Conference on Signals, Systems & Computers*, Pacific Grove, CA, USA, Oct. 1992.

[35] J. Ward, A.O. Steinhardt, "Multiwindow post-Doppler space-time adaptive processing," *IEEE 7th Workshop on Statistical Signal and Array Processing*, Quebec City, QC, Canada, June 1994.

[36] J.K. Day, F.M. Staudaher, "Airborne MTI," in *Radar Handbook*, *3rd ed.*, M. Skolnik, editor, McGraw-Hill, 2008.

[37] J.B. Billingsley, A. Farina, F. Gini, M.V. Greco, L. Verrazzani, "Statistical analyses of measured radar ground clutter data," *IEEE Trans. Aerospace & Electronic Systems*, vol. 35, no. 2, pp. 579-593, Apr 1999.

[38] J.G. Metcalf, K.J. Sangston, M. Rangaswamy, S.D. Blunt, B. Himed, "A new method of generating multivariate Weibull distributed data," *IEEE Radar Conf.* Philadelphia, PA, USA, May 2016.

[39] S.D. Blunt, M. Cook, J. Jakabosky, J.D. Graaf, E. Perrins, "Polyphase-coded FM (PCFM) radar waveforms, part I: implementation," *IEEE Trans. Aerospace & Electronic Systems*, vol. 50, no. 3, pp. 2218-2229, July 2014.

[40] S.D. Blunt, J. Jakabosky, M. Cook, J. Stiles, S. Seguin, E. Mokole, "Polyphase-coded FM (PCFM) radar waveforms, part II: optimization," *IEEE Trans. Aerospace & Electronic Systems*, vol. 50, no. 3, pp. 2230-2241, July 2014.